Author(s): Civitarese, O.; Suhonen, Jouni

Title: Strength of J(pi)=1(+) Gamow-Teller and isovector spin monopole transitions in double-beta-decay triplets

Year: 2014

Version:

Please cite the original version:

Civitarese, O., & Suhonen, J. (2014). Strength of J(pi)=1(+) Gamow-Teller and isovector spin monopole transitions in double-beta-decay triplets. Physical Review C, 89(4), Article 044319. https://doi.org/10.1103/PhysRevC.89.044319

Strength of $J^\pi = 1^+$ Gamow-Teller and isovector spin monopole transitions in double-β-decay triplets

O. Civitarese[1] and J. Suhonen[2]

[1]*Departamento de Física, Universidad Nacional de La Plata, C.C. 67, 1900 La Plata, Argentina*

[2]*University of Jyväskylä, Department of Physics, P.O. Box 35 (YFL), FI-40014 Jyväskylä, Finland*

(Received 20 February 2014; revised manuscript received 4 April 2014; published 18 April 2014)

In this work we study systematically the energetics and intensity distributions of Gamow-Teller ($GT^\pm$) and isovector spin monopole ($IVSM^\pm$) transitions from the ground states of the pairs (^{76}Ge,^{76}Se), (^{82}Se,^{82}Kr), (^{100}Mo,^{100}Ru), (^{116}Cd,^{116}Sn), (^{128}Te,^{128}Xe), (^{130}Te,^{130}Xe), and (^{136}Xe,^{136}Ba), of double-beta-decay initial and final nuclei, to the $J^\pi = 1^+$ excited states of the intermediate odd-odd nuclei ^{76}As, ^{82}Br, ^{100}Tc, ^{116}In, ^{128,130}I, and ^{136}Cs. We use a proton-neutron quasiparticle random-phase approximation (QRPA) theory framework with the Bonn-A two-body interaction in large no-core single-particle valence bases. Our studies indicate that the GT^- strength at the giant resonance (GTGR) region and the low-energy part of the $IVSM^-$ strength overlap, which could be of significance for the analyses of the (p,n) type of reaction experiments at and around the GTGR.

DOI: 10.1103/PhysRevC.89.044319 PACS number(s): 21.60.Jz, 23.40.Bw, 23.40.Hc, 27.50.+e

I. INTRODUCTION

Theoretical study of the nuclear-structure properties of double-beta-decay emitters is one of the most challenging activities in the field of nuclear physics, and it is of utmost relevance for the analysis and design of experiments [1,2]. Analyses of the related nuclear matrix elements (NMEs) have mostly been performed within the framework of the proton-neutron quasiparticle random-phase approximation (pnQRPA) or some higher order variant of it (see, e.g., [3]). However, many other models have also been used earlier [2] and new models have joined recently [4]. Among the various nuclear-structure aspects related to double-beta-decay studies, some attention has been recently paid to detailed comparisons between experimental results of single-beta decay and charge-exchange-reaction data and theoretical calculations of the energy distribution of the intensity for allowed Gamow-Teller transitions (see, e.g., [5]).

Low-energy and high-energy Gamow-Teller (GT) strength distributions are a very useful tool to access the validity of various theoretical assumptions and approximations, such as the sequences of single-particle states, the values of the level occupancies, and the sizes of the model spaces used to perform calculations (see, e.g., [6–8]). Here we shall focus on the systematics of the excitation of the isovector spin monopole (IVSM) mode. In a first investigation on the subject [9] we addressed the question of the interplay between the IVSM and Gamow-Teller (GT) modes in the context of a schematic model, and tested its results by performing realistic pnQRPA calculations. In this work we extend our search to some of the most favored double-beta-decay emitters in order to extract some conclusions about the energetics, strength distributions, and mass dependence of total intensities of the $IVSM^\mp$ modes in the (p,n) and (n,p) charge-exchange directions.

In Sec. II we give a brief introduction to the underlying formalism of the GT and IVSM modes of excitation and in Sec. III we display and discuss the obtained results. The final conclusions are drawn in Sec. IV.

II. BRIEF REVIEW OF THE FORMALISM

The formalism developed in [9] is now applied to calculate the nuclear response to the excitation of Gamow-Teller (GT) and isovector spin monopole (IVSM) modes, starting from the ground states of few selected even-even nuclei. For the present study we have chosen the double-beta-decay emitters in the $A = 76$, $A = 82$, $A = 100$, $A = 116$, $A = 128$, $A = 130$, and $A = 136$ triplets of isobars, in order to perform a case-by-case analysis of the transitions. In particular, we aim at the identification of the IVSM strength at low energies because of the potentially important implications upon nuclear double-beta-decay studies [10–16]. The main steps of the calculations are the following:

(i) Single-particle bases: We build the single-particle bases for each involved nucleus by solving the radial Schrödinger equation for a Coulomb-corrected Woods-Saxon potential by starting from the $nl_j = 0s_{1/2}$ state (no-core basis), for both protons and neutrons. We use the Woods-Saxon parameters given in [17]. We deal with bound states and quasibound states only. Extra care has to be taken when dealing with the quasibound states near the top of the angular-momentum and centrifugal barriers. These cases can be dealt with by very carefully choosing the iteration increment of the solver for unbound states. The sequence of levels is adjusted, when possible, to correspond to the observed sequence of single-particle states and/or the known experimental occupancies of the key orbits of calculation. These adjustments affect the values of monopole pairing strengths, pairing gaps, quasiparticle energies, occupancies of orbitals, etc., as explained next.

(ii) Pairing gaps, quasiparticle energies, and BCS occupancy factors: The two-body potential used in the calculations was derived from the Bonn-A one-boson-exchange potential [18]. The monopole pairing strength was fixed by fitting the BCS gaps to the observed odd-even mass differences [19–21]. We

tabulate the values of the pairing strength constants and the obtained proton and neutron gaps in the next section.

(iii) Spectra of the 1^+ excitations in odd-odd nuclei: The wave functions and energies, for the complete set of 1^+ excitations in the odd-odd nuclei, were obtained by performing a pnQRPA diagonalization in the space of unperturbed quasiproton-quasineutron pairs coupled to $J^\pi = 1^+$. The formalism is well known and we shall skip the details here (see, e.g., [19,21]). In the tables of the next section we give for each mass system the values of the relevant parameters, i.e., strengths of the particle-hole and particle-particle interactions used in the calculations.

(iv) Transition operators and strength distributions for the GT and IVSM excitations: The transition operators are written in terms of quasiproton-quasineutron pairs and further transformed to the pnQRPA basis by expressing the transition densities in terms of one-phonon variables.

The final expressions for the relevant transition matrix elements, connecting the initial ground state with the kth 1^+ state, read [9,19]

$$\langle 1^+_m \| \sum_k \mathrm{O_1(k)t^\pm_k} \| 0^+ \rangle = \sum_{p,n} \frac{\langle p \,||\, \mathrm{O_1} \,||\, \mathrm{n} \rangle}{\sqrt{3}} \left(u_p v_n X^m_{pn} + u_n v_p Y^m_{pn} \right), \quad (1)$$

where X^m_{pn} and Y^m_{pn} are the forward- and backward-going amplitudes of the state with energy E_m. Furthermore, u and v are the BCS vacancy and occupancy factors, respectively. The GT and IVSM operators are defined as

$$\mathrm{O}_{1\mu} t^\pm(\mathrm{GT}) = \sigma_{1\mu} t^\pm, \qquad \mathrm{O}_{1\mu} t^\pm(\mathrm{IVSM}) = \sigma_{1\mu} r^2 t^\pm. \quad (2)$$

and the strength S, for each operator, is given by the sum over all 1^+ states belonging to the spectrum of the daughter odd-odd mass nucleus, such that

$$S_\pm = \sum_{m,\mu} |\langle 1^+_m \, \mu | \sum_k \mathrm{O}_{1\mu}(k) t^\pm_k | 0^+ \rangle|^2. \quad (3)$$

For the GT operator the difference between the total intensities of the two branches of excitation gives the standard Ikeda sum rule, $S_-(\mathrm{GT}) - S_+(\mathrm{GT}) = 3(N - Z)$, which is model independent and which is fulfilled if both members of the spin-orbit pairs corresponding to a given value of the single-particle orbital angular momentum are included in the basis [19]. This sum rule is preserved quite accurately by all the present pnQRPA calculations. For the IVSM mode there is no model-independent sum rule due to the radial dependence of the operator, but it is possible to extract a limit for it, in the chosen model space for calculations, by shifting the IVSM operator with the excess square radius $\langle r^2 \rangle_{\mathrm{excess}}$ [22], defined as the average over the excess neutron orbits. By this procedure the appropriate IVSM strength is obtained by the use of the shifted operator

$$r^2 \to r^2 - \langle r^2 \rangle_{\mathrm{excess}}. \quad (4)$$

We use this prescription to obtain the IVSM$^-$ and IVSM$^+$ strength distributions discussed in Sec. III.

TABLE I. Adopted neutron and proton single-particle states and their energies for the mass $A = 76$ system. The energies are given in units of MeV.

Proton orbitals and energies			Neutron orbitals and energies		
nl_j	^{76}Ge	^{76}Se	nl_j	^{76}Ge	^{76}Se
$0s_{1/2}$	−36.17	−33.80	$0s_{1/2}$	−37.86	−39.51
$0p_{3/2}$	−29.59	−27.33	$0p_{3/2}$	−31.12	−32.69
$0p_{1/2}$	−28.07	−25.83	$0p_{1/2}$	−29.86	−31.41
$0d_{5/2}$	−22.12	−19.96	$0d_{5/2}$	−23.61	−25.10
$0d_{3/2}$	−18.74	−16.64	$0d_{3/2}$	−20.79	−22.21
$1s_{1/2}$	−18.16	−16.06	$1s_{1/2}$	−20.35	−21.80
$0f_{7/2}$	−13.97	−11.93	$0f_{7/2}$	−15.52	−16.91
$1p_{3/2}$	−9.01	−7.00	$1p_{3/2}$	−11.52	−12.77
$0f_{5/2}$	−8.21	−6.29	$0f_{5/2}$	−10.72	−11.98
$1p_{1/2}$	−6.79	−5.00	$1p_{1/2}$	−9.80	−10.98
$0g_{9/2}$	−5.31	−3.37	$0g_{9/2}$	−7.03	−8.30
$1d_{5/2}$	−0.27	1.37	$1d_{5/2}$	−3.30	−4.29
$2s_{1/2}$	1.61	2.96	$2s_{1/2}$	−2.17	−2.94
$0g_{7/2}$	3.05	4.73	$1d_{3/2}$	−0.80	−1.58
$1d_{3/2}$	3.07	4.45	$0g_{7/2}$	−0.18	−1.20
$0h_{11/2}$	3.70	5.44	$2p_{3/2}$	1.59	3.95
$1f_{7/2}$	7.25	8.60	$0h_{11/2}$	1.65	0.54
$0i_{13/2}$	10.40	10.40	$1f_{7/2}$	3.50	2.62
			$0h_{9/2}$	9.95	9.17
			$0i_{13/2}$	10.14	9.23
			$1f_{5/2}$	10.60	10.60

III. RESULTS AND DISCUSSION

In this section we present and discuss the results of the calculations. For the sake of completeness we shall introduce each of the elements entering the calculations, referring to the already published material for details.

A. Single-particle bases and energies

The single-particle energies are the eigenstates of the Woods-Saxon potential (adding Coulomb force for protons) and we keep bound and quasibound states, e.g., eigenstates with very small decay width. The parameters of the central, orbital, and spin-orbit terms of the potential, as well as the radius and surface thickness parameters for each term, are taken from [17]. Since these are no-core calculations, we are taking all orbits from the $N = 0$ oscillator shell up to two oscillator major shells above the respective Fermi surfaces for protons and neutrons in each system. For the $A = 82, 116, 130, 136$ isobars the Woods-Saxon single-particle energies work well, but for the $A = 100$ isobars we have

TABLE II. Pairing scaling factors and the resulting pairing gaps, given in units of MeV. For the $A = 76$ nuclei "WS + BCS" denotes the Woods-Saxon based and "exp" the experiment-based occupancies. For ^{116}Sn (^{136}Xe) the proton (neutron) pairing strength is adopted from ^{116}Cd (^{136}Ba) since there is no proton (neutron) pairing gap for ^{116}Sn (^{136}Xe) due to its proton (neutron) magicity.

Nucleus	$g_{\rm pair}^{(\rm n)}$	$g_{\rm pair}^{(\rm p)}$	$\Delta_{\rm n}$ (MeV)	$\Delta_{\rm p}$ (MeV)
^{76}Ge (WS + BCS)	1.01	0.89	1.57	1.51
^{76}Se (WS + BCS)	1.02	0.91	1.72	1.71
^{76}Ge (exp)	0.82	0.87	1.57	1.51
^{76}Se (exp)	0.89	0.84	1.72	1.71
^{82}Se	1.00	0.83	1.51	1.39
^{82}Kr	1.07	0.86	1.65	1.64
^{100}Mo	0.85	0.89	1.25	1.37
^{100}Ru	0.89	0.96	1.40	1.48
^{116}Cd	0.89	0.94	1.37	1.48
^{116}Sn	0.82	0.94	1.16	
^{128}Te	0.86	0.81	1.29	1.09
^{128}Xe	0.86	0.87	1.27	1.29
^{130}Te	0.94	0.80	1.20	1.00
^{130}Xe	0.95	0.86	1.25	1.27
^{136}Xe	0.90	0.74		0.925
^{136}Ba	0.90	0.83	1.08	1.23

to resort to the "EXPWS" energies of Ref. [23] and for the $A = 128$ isobars we use the basis introduced in [5].

For the $A = 76$ isobars we can use two prescriptions. In Table I we show for the mass $A = 76$ system the values of single-particle energies of protons and neutrons for the Woods-Saxon potential, adopted as input for the calculation of the occupancies and quasiparticle spectra in this work. Furthermore, we compare the results emerging from these occupancies and quasiparticle energies with those emerging from the experimentally measured proton and neutron occupancies [24,25] at the respective Fermi surfaces. These experimental occupancies were already used in the works [6–8,26]. The information about the single-particle levels and their energies for the mass $A = 100$, $A = 116$, and $A = 128$ systems has been given in Ref. [5], in Tables 2 and 3.

As already mentioned, we can adopt for the mass $A = 76$ case the measured occupancies of Refs. [24,25]. To cope with the experimental occupancies one can take as a starting point the Woods-Saxon energies of Table I and perform the usual BCS calculation, after which one subsequently replaces manually the computed occupancies with the measured ones close to the proton and neutron Fermi surfaces. These partly modified occupancies are not quite consistent with the underlying BCS calculation, but it was shown in [6] that the resulting average proton and neutron numbers correspond quite accurately to the

TABLE III. Renormalization factors for the particle-hole and particle-particle interactions in the $J^\pi = 1^+$ channel, and the energy of the first pnQRPA eigenvalue (in MeV) relative to the ground state of the mother nucleus. Also are given the excess radii used to compute the IVSM$^-$ and IVSM$^+$ strength distributions by the prescription (4). For the $A = 76$ nuclei "WS + BCS" denotes the Woods-Saxon-based and "exp" the experiment-based occupancies adopted in the calculations.

Mother nucleus	$g_{\rm ph}$	$g_{\rm pp}$	$E(1_1^+)$	$\langle r^2\rangle_{\rm excess}$ (fm^2)
^{76}Ge (WS + BCS)	1.00	0.63	4.662	16.95
^{76}Se (WS + BCS)	1.00	0.63	4.100	16.90
^{76}Ge (exp)	1.00	0.63	3.087	16.95
^{76}Se (exp)	1.00	0.63	3.044	16.90
^{82}Se	1.00	0.63	4.978	17.55
^{82}Kr	1.00	0.63	4.685	17.52
^{100}Mo	0.90	0.63	3.479	19.67
^{100}Ru	0.90	0.63	3.507	19.85
^{116}Cd	1.00	0.63	3.052	21.55
^{116}Sn	1.00	0.63	2.515	22.21
^{128}Te	1.00	0.63	2.456	23.17
^{128}Xe	1.00	0.63	2.556	23.18
^{130}Te	1.00	0.63	3.434	23.21
^{130}Xe	1.00	0.63	3.308	23.22
^{136}Xe	1.00	0.63	3.247	23.88
^{136}Ba	1.00	0.63	4.628	23.89

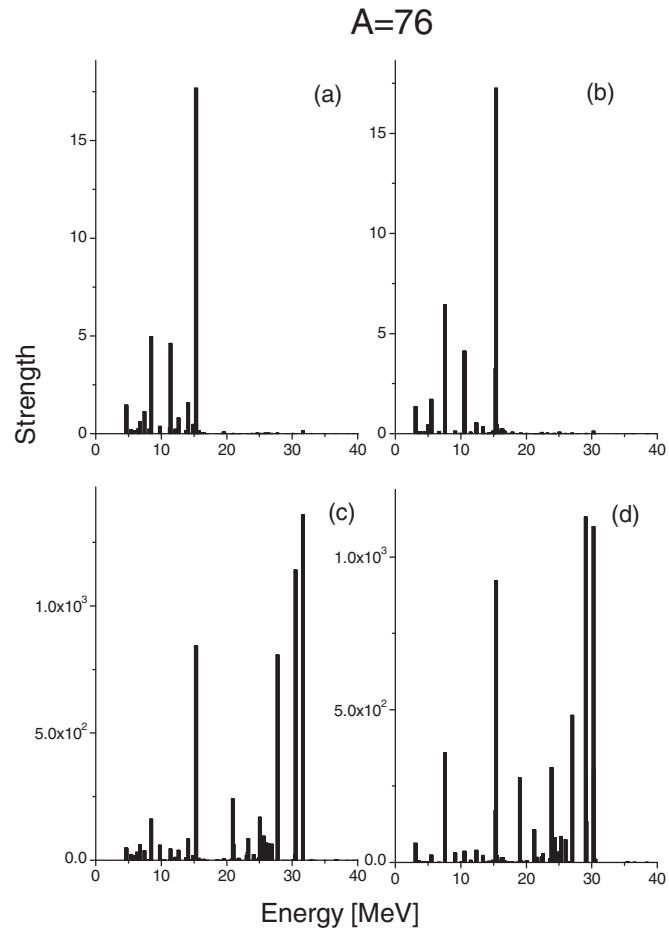

FIG. 1. Distribution of the GT$^-$ [panels (a) and (b)] and IVSM$^-$ [panels (c) and (d)] strength, (6) and (8), in the transition ^{76}Ge $\rightarrow$ ^{76}As. The excitation energies are measured from the ground state of ^{76}Ge. The IVSM strength is given in units of fm^4. The occupancies of the single-particle orbitals are based on either the WS + BCS model (left panels) or on experiment (right panels).

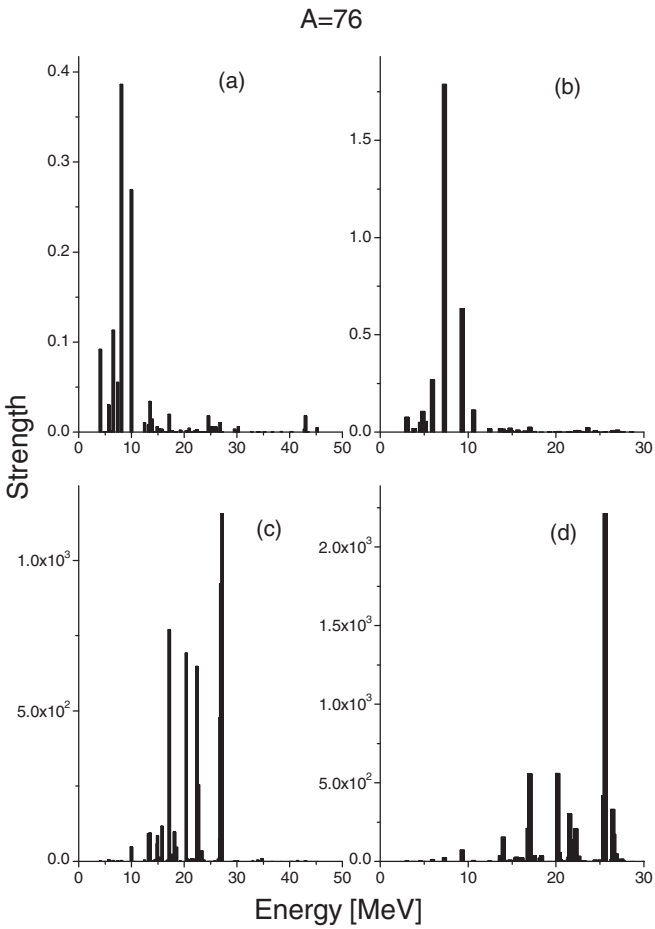

FIG. 2. Distribution of the GT^+ [panels (a) and (b)] and $IVSM^+$ [panels (c) and (d)] strength, (7) and (9), in the transition $^{76}Se \rightarrow {}^{76}As$. The excitation energies are measured from the ground state of ^{76}Se. The IVSM strength is given in units of fm^4. The occupancies of the single-particle orbitals are based on either the WS + BCS model (left panels) or on experiment (right panels).

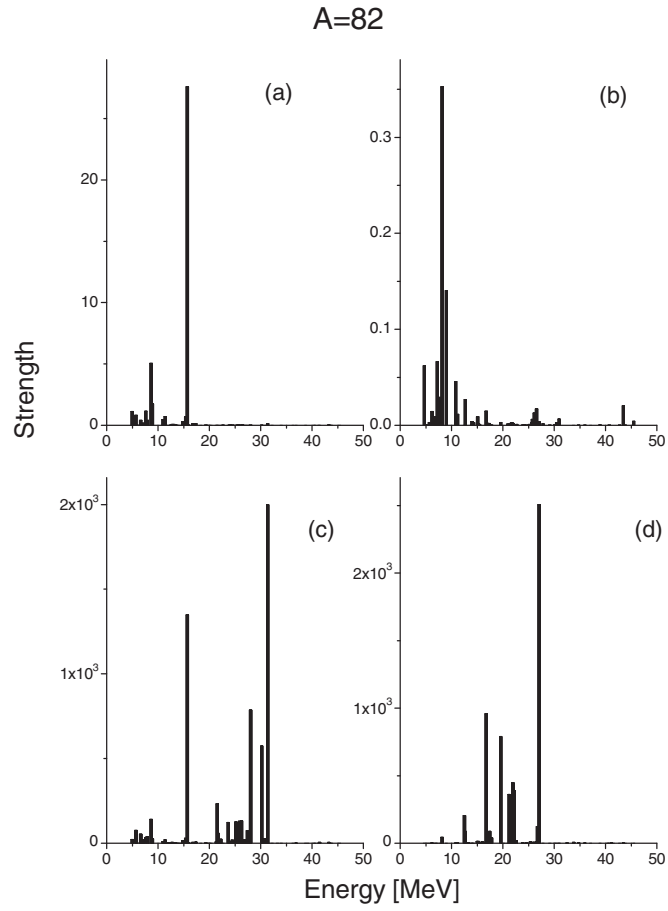

FIG. 3. Distribution of the GT^- [panel (a)], GT^+ [panel (b)], $IVSM^-$ [panel (c)], and $IVSM^+$ [panel (d)] strength, (6), (7), (8), and (9), in the transitions $^{82}Se \rightarrow {}^{82}Br$ [panels (a) and (c)] and $^{82}Kr \rightarrow {}^{82}Br$ [panels (b) and (d)]. The excitation energies are measured from the ground state of ^{82}Se for GT^- and $IVSM^-$, and from the ground state of ^{82}Kr for GT^+ and $IVSM^+$. The IVSM strength is given in units of fm^4.

actual numbers of protons and neutrons in the ^{76}Ge and ^{76}Se nuclei. The occupancies then determine the theoretical pairing gaps and quasiparticle energies, and the quasiparticle energies in turn, together with the occupancies, determine uniquely the results of the pnQRPA equations of motion.

B. Pairing gaps, quasiparticle spectra, and BCS occupation factors

The monopole two-body matrix elements generated from the Bonn-A interaction were adapted to finite nuclei by an overall renormalization of the strength of the monopole proton and neutron channels, separately. The corresponding scaling factor for neutrons (protons) is denoted by $g_{\rm pair}^{\rm (n)}$ ($g_{\rm pair}^{\rm (p)}$), and its adopted values are tabulated in column two (column three) of Table II. With the tabulated scaling factors the BCS-calculated pairing gaps reproduce the empirically deduced gaps that are tabulated in columns four and five of Table II. Using the tabulated scaling factors we have performed BCS calculations to obtain the one-quasiparticle energies and occupation factors needed to perform the subsequent pnQRPA calculations.

The occupancies, for the cases in which they have been determined experimentally, as in the case of the $A = 76$ system, are valuable indicators of the reliability of the adopted single-particle energies [6,26]. In addition to the systematics on the observed odd-even mass differences, the adjustment of the single-particle energies [23,27–30] reduces the tension with the data concerning low-lying quasiparticle excitations in the adjacent odd-mass nuclei. The different adjustment schemes and the resulting occupation amplitudes have been tabulated extensively for ^{76}Ge, ^{76}Se, ^{130}Te, and ^{130}Xe in Tables 1–4 of [6]. In the present work we exploit the "WS + BCS" and experimental schemes of these tables for $A = 76$ and the Woods-Saxon scheme for $A = 130$. For the $A = 100$, $A = 116$, and $A = 128$ systems the occupancies (occupation amplitudes squared times the degeneracies of the j orbitals) at the respective Fermi surfaces have been tabulated in Ref. [5], in Tables 5, 6, and 7.

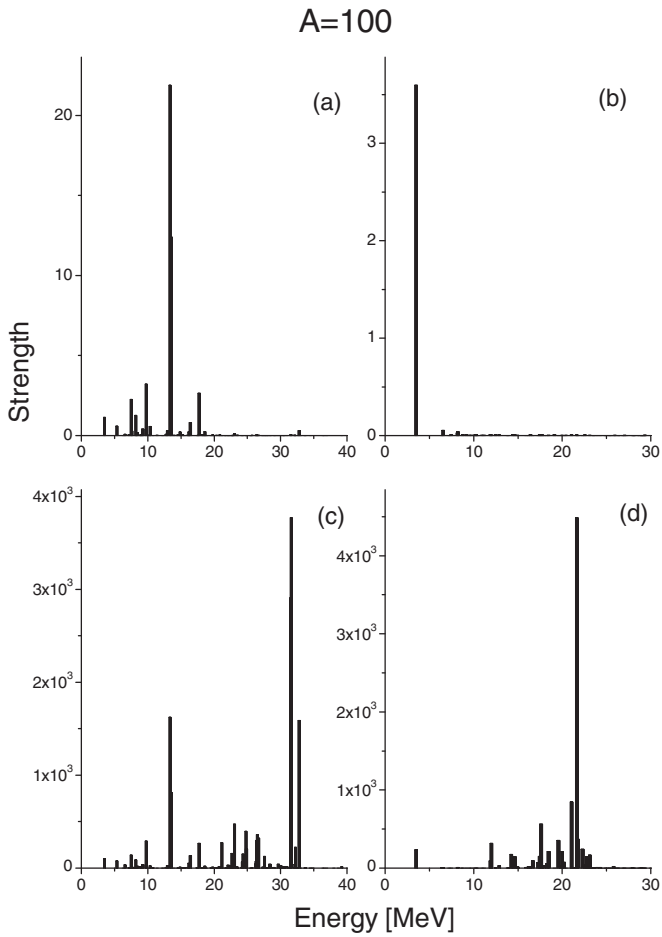

FIG. 4. Distribution of the GT^- [panel (a)], GT^+ [panel (b)], $IVSM^-$ [panel (c)], and $IVSM^+$ [panel (d)] strength, (6), (7), (8), and (9), in the transitions $^{100}Mo \rightarrow {}^{100}Tc$ [panels (a) and (c)] and $^{100}Ru \rightarrow {}^{100}Tc$ [panels (b) and (d)]. The excitation energies are measured from the ground state of ^{100}Mo for GT^- and $IVSM^-$, and from the ground state of ^{100}Ru for GT^+ and $IVSM^+$. The IVSM strength is given in units of fm^4.

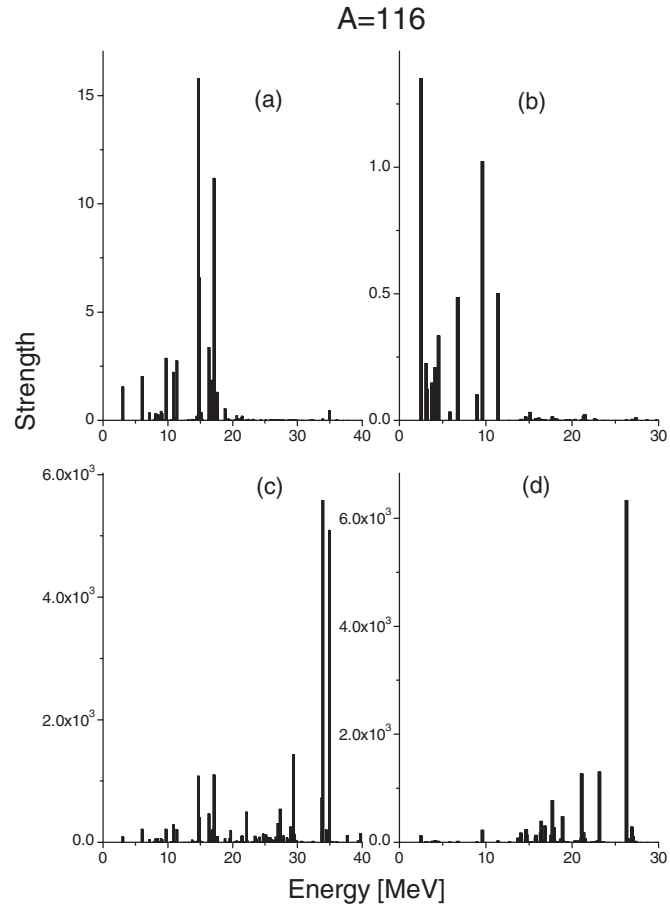

FIG. 5. Distribution of the GT^- [panel (a)], GT^+ [panel (b)], $IVSM^-$ [panel (c)], and $IVSM^+$ [panel (d)] strength, (6), (7), (8), and (9), in the transitions $^{116}Cd \rightarrow {}^{116}In$ [panels (a) and (c)] and $^{116}Sn \rightarrow {}^{116}In$ [panels (b) and (d)]. The excitation energies are measured from the ground state of ^{116}Cd for GT^- and $IVSM^-$, and from the ground state of ^{116}Sn for GT^+ and $IVSM^+$. The IVSM strength is given in units of fm^4.

C. Spectra of the 1^+ excitations in odd-odd nuclei and the GT and IVSM transitions

For each of the isobaric systems with mass number A we have taken the triplet to be composed of "left-hand-side" even-even (A,N,Z), "right-hand-side" even-even $(A,N-2,Z+2)$, and "intermediate" odd-odd $(A,N-1,Z+1)$ nuclei. The spectra of 1^+ excitations, belonging to the odd-odd mass nuclei, were constructed by applying the pnQRPA formalism [20,21,31], including particle-hole and particle-particle channels in the residual (proton-neutron) two-body interactions. The linearization procedure yields, therefore, two sets of energies and wave functions of 1^+ states which are reached by the action of the t^- and t^+ components of the GT and IVSM operators from the ground states of the left-hand-side and right-hand-side nuclei, respectively. Table III shows the values of the particle-hole renormalization factors g_{ph} which roughly reproduce the energetics of the GT^- giant resonance (GTGR). In the table we list also the values of the particle-particle renormalization factor g_{pp} and the energies of the first excited 1^+ state obtained by applying the pnQRPA formalism starting from the left and right ground states of the double-even mass nuclei of each mass system.

While the value of g_{ph} is determined by the properties of the GTGR, the value of the particle-particle parameter g_{pp} is not so easily pinned down. Typically its value has been fixed either by the half-lives of $2\nu\beta\beta$ decays [32–36] or the comparative half-lives ($\log ft$ values) of beta decays [27,37]. In [5,38] a novel approach was introduced where both beta-decay and $2\nu\beta\beta$-decay data was used to determine both the value of g_{pp} and the (effective) value of the axial-vector coupling constant $g_A(\beta)$ simultaneously. From the analysis of [5] we can extract the following average values of these quantities:

$$\langle g_{pp} \rangle = 0.63 \pm 0.17, \quad \langle g_A(\beta) \rangle = 0.57 \pm 0.21. \qquad (5)$$

We adopt the above value of the particle-particle coupling strength to our further analyses of the GT and IVSM properties of the discussed triplets of isobars listed in Table III.

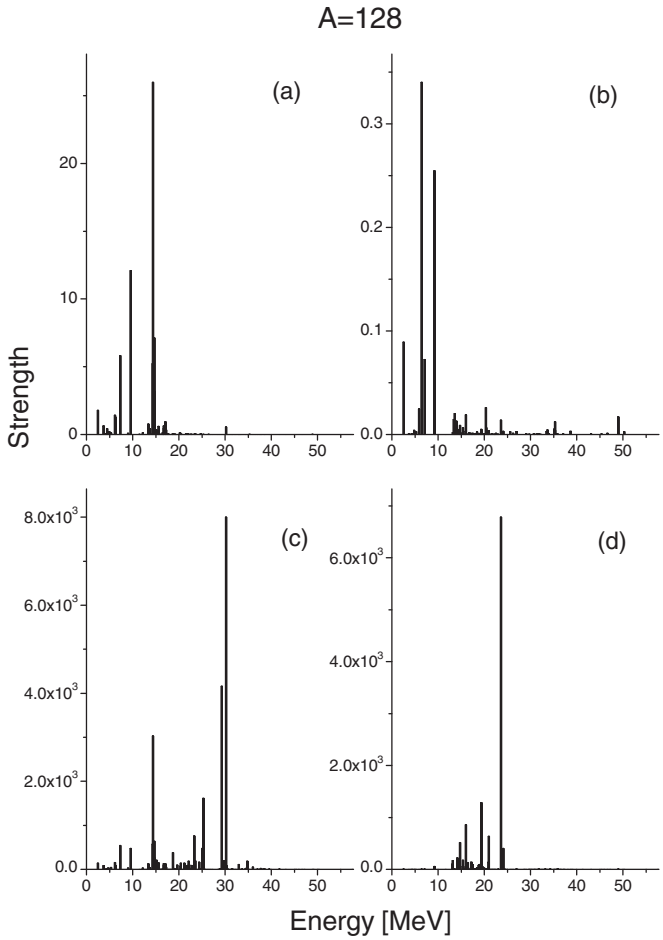

FIG. 6. Distribution of the GT$^-$ [panel (a)], GT$^+$ [panel (b)], IVSM$^-$ [panel (c)], and IVSM$^+$ [panel (d)] strength, (6), (7), (8) and (9), in the transitions ^{128}Te $\rightarrow$ ^{128}I [panels (a) and (c)] and ^{128}Xe $\rightarrow$ ^{128}I [panels (b) and (d)]. The excitation energies are measured from the ground state of ^{128}Te for GT$^-$ and IVSM$^-$, and from the ground state of ^{128}Xe for GT$^+$ and IVSM$^+$. The IVSM strength is given in units of fm^4.

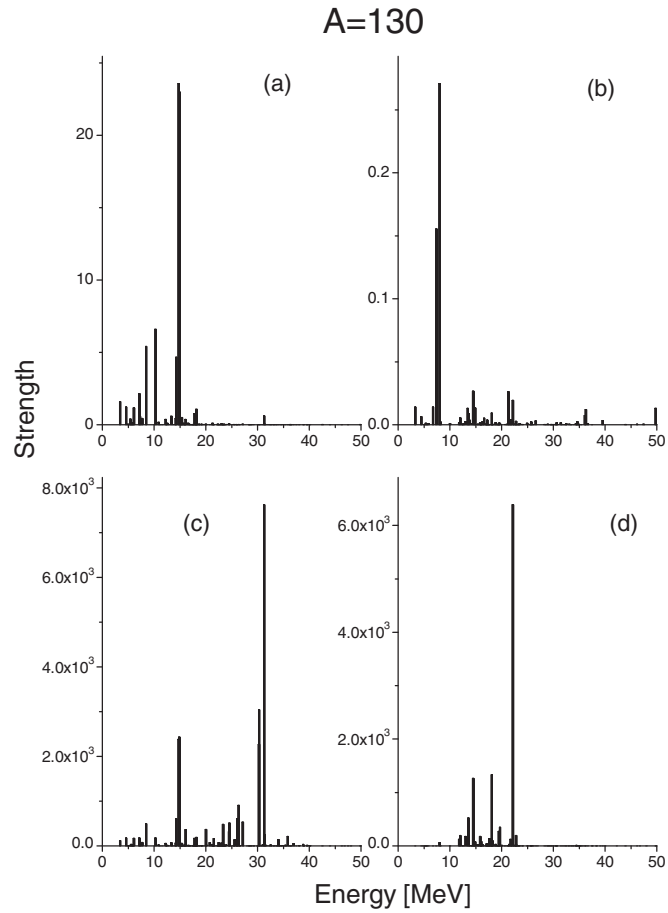

FIG. 7. Distribution of the GT$^-$ [panel (a)], GT$^+$ [panel (b)], IVSM$^-$ [panel (c)], and IVSM$^+$ [panel (d)] strength, (6), (7), (8) and (9), in the transitions ^{130}Te $\rightarrow$ ^{130}I [panels (a) and (c)] and ^{130}Xe $\rightarrow$ ^{130}I [panels (b) and (d)]. The excitation energies are measured from the ground state of ^{130}Te for GT$^-$ and IVSM$^-$, and from the ground state of ^{130}Xe for GT$^+$ and IVSM$^+$. The IVSM strength is given in units of fm^4.

D. Strength functions for the GT and IVSM excitations

Here we discuss the distributions of the GT and IVSM strength for the left-hand-side (GT$^-$ and IVSM$^-$) and right-hand-side (GT$^+$ and IVSM$^+$) initial ground states. We then have the GT$^-$ and IVSM$^-$ transitions ^{76}Ge $\rightarrow$ ^{76}As, ^{82}Se $\rightarrow$ ^{82}Br, ^{100}Mo $\rightarrow$ ^{100}Tc, ^{116}Cd $\rightarrow$ ^{116}In, ^{128}Te $\rightarrow$ ^{128}I, ^{130}Te $\rightarrow$ ^{130}I, and ^{136}Xe $\rightarrow$ ^{136}Cs, and the GT$^+$ and IVSM$^+$ transitions ^{76}Se $\rightarrow$ ^{76}As, ^{82}Kr $\rightarrow$ ^{82}Br, ^{100}Ru $\rightarrow$ ^{100}Tc, ^{116}Sn $\rightarrow$ ^{116}In, ^{128}Xe $\rightarrow$ ^{128}I, ^{130}Xe $\rightarrow$ ^{130}I, and ^{136}Ba $\rightarrow$ ^{136}Cs. We then have the strength functions

$$B(\mathrm{GT})_-(m) = \left|(1^+_m\|\sum_k t^-_k\boldsymbol{\sigma}_k\|0^+_\mathrm{L})\right|^2, \quad (6)$$

$$B(\mathrm{GT})_+(m) = \left|(1^+_m\|\sum_k t^+_k\boldsymbol{\sigma}_k\|0^+_\mathrm{R})\right|^2, \quad (7)$$

$$B(\mathrm{IVSM})_-(m) = \left|(1^+_m\|\sum_k t^-_k r^2_k\boldsymbol{\sigma}_k\|0^+_\mathrm{L})\right|^2, \quad (8)$$

$$B(\mathrm{IVSM})_+(m) = \left|(1^+_m\|\sum_k t^+_k r^2_k\boldsymbol{\sigma}_k\|0^+_\mathrm{R})\right|^2, \quad (9)$$

where 0^+_L (0^+_R) is the ground state of the left-hand-side (right-hand-side) even-even nucleus and 1^+_m is the mth 1^+ state in the intermediate nucleus. These strength functions are illustrated in Figs. 1–8. In Figs. 1 and 2 the left panels show the results based on the WS + BCS occupancies, whereas the right panels show the results based on BCS occupancies supplemented with the experimental occupancies for the key orbitals at the proton and neutron Fermi surfaces.

There is a possibility to compare the presently computed GT$^-$ and GT$^+$ distributions with the corresponding experimental ones [13] for the $A = 76$ case. The experimental GT$^-$ distribution is conveniently displayed in the uppermost panel

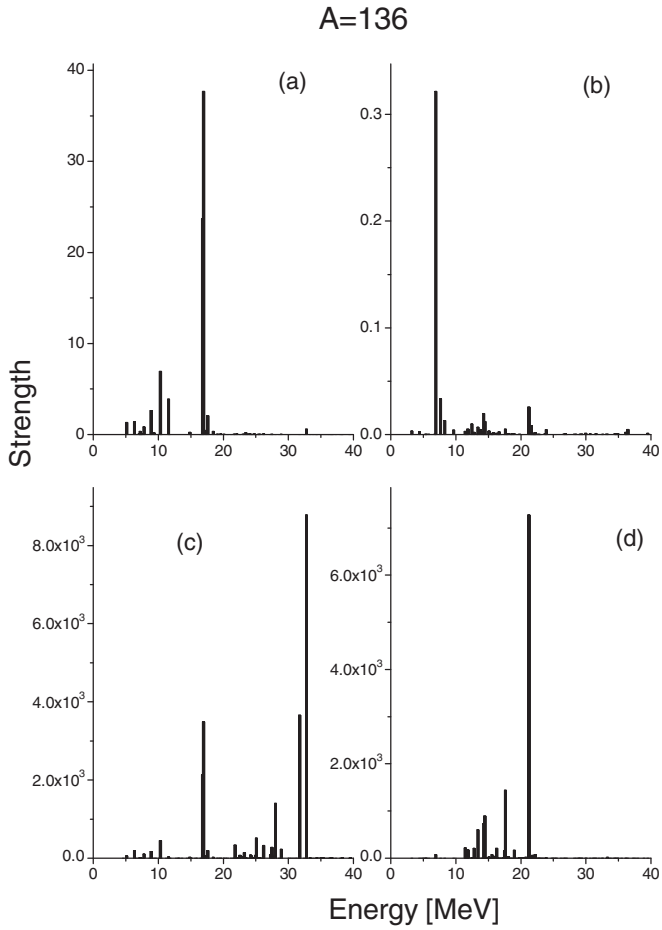

FIG. 8. Distribution of the GT^- [panel (a)], GT^+ [panel (b)], $IVSM^-$ [panel (c)], and $IVSM^+$ [panel (d)] strength, (6), (7), (8) and (9), in the transitions $^{136}Xe \rightarrow {}^{136}Cs$ [panels (a) and (c)] and $^{136}Ba \rightarrow {}^{136}Cs$ [panels (b) and (d)]. The excitation energies are measured from the ground state of ^{136}Xe for GT^- and $IVSM^-$, and from the ground state of ^{136}Ba for GT^+ and $IVSM^+$. The IVSM strength is given in units of fm^4.

of Fig. 1 of [39] and the GT^+ distribution in the uppermost panel of Fig. 3 of the same article. When comparing the left and right upper panels of our present Fig. 1 with the experimental GT^- distribution [39], one notices a great similarity of the experimental and computed distributions: there are two strong peaks below 10 MeV of relative excitation energy (i.e., relative to the energy of the first 1^+ state) both in the calculated and in the experimental distributions, in addition to the strong GTGR peak at around 11–12 MeV of relative excitation. It seems that both the "WS" and "exp" based calculations reproduce the gross features of the experimental GT^- distribution rather well. Comparing the experimental and theoretical GT^+ distributions one notices that the "WS" based calculation reproduces the strength of the experimental distribution but is twice as broad as it. The "exp" based calculation has too much GT^+ strength at low energies. Also for the $A = 100$ and $A = 128$ cases the computed GT^- distributions agree nicely with the experiments as seen in Tables 10 and 12 of [5].

At this point it is worth noting that, with respect to the two-neutrino double-beta decays, the decay of ^{116}Cd shows single-state dominance [40,41], as clearly shown in Fig. 3 of [5]. Instead, the decay ^{100}Mo is not quite single-state dominated (see Fig. 3 of [5]) and the decay of ^{128}Te not at all as seen in Fig. 4 of [5]. The decays of ^{76}Ge, ^{82}Se, ^{130}Te, and ^{136}Xe are not single-state dominated, as seen from the sizable overlap of the GT^- and GT^+ strengths in Figs. 1–3, 7, and 8.

E. Energy centroids and total and peak intensities of the GT and IVSM modes

In Tables IV–VII we show the results for the calculated energy centroids, both for $GT^\pm$ and $IVSM^\pm$ transitions, as well as the energies and intensities of the states which carry the largest strength for each type of operator. The overall feature which emerges from these results is pretty consistent with the model estimates of our previous work [9]; that is, (a) the fraction of the total intensity carried by the state with the largest intensity is roughly the same for GT^- and $IVSM^-$ modes (which is approximately 20–30 % of the strength), and (b) the energy difference between the two energy centroids (as also between the states with the largest intensities) is of the order of $2\hbar\omega$. Concerning the mass dependence of the right-hand side of the transitions, the results for the $IVSM^+$ mode are very much concentrated around energies of the order of 20–25 MeV, while the intensities of the GT^+ tend to be dominated by few states in the low-energy part of the spectrum.

As seen in Figs. 1–8, there is also a visible mismatch between the branches of the GT^- and GT^+ excitations at the GTGR energies, indicating that there are practically no contributions to the $2\nu\beta\beta$ NME that stem from the GTGR region and beyond. This was shown tangibly for the $A = 100$, $A = 116$, and $A = 128$ double-beta systems in [5] by recording cumulative sums of the $2\nu\beta\beta$ NMEs. The other interesting feature concerning the IVSM modes is the appearance of significant strength, for the $IVSM^-$ side of the transitions, at energies of the order of 10–20 MeV where also the GT^- giant resonance appears. This happens consistently for all the considered triplets of isobars. For example, for ^{76}Ge there is an exact match of the $IVSM^-$ and GT^- strengths at the largest (two largest) GT^- peaks for the "WS + BCS" occupancies ("exp" occupancies) in the left (right) panel of Fig. 1. For ^{100}Mo there is an exact match at the GT^- peak energy (Fig. 4) and for ^{116}Cd a number of matching strengths for the GT^- peaks between 14 and 17 MeV, as seen in Fig. 5. In these cases the interaction between both modes may be possible.

The matching of the GT^- peaks and $IVSM^-$ peaks around the GTGR region is further studied systematically in Table VIII, where we show the amplitudes of transitions to 1^+ states around the GTGR, for which the magnitude of the GT^- amplitude is larger than unity. These transitions constitute the most important contributions to the GT^- and $IVSM^-$ strengths around the GTGR region. As seen from the table, the ratio between the $IVSM^-$ amplitudes (expressed in fm^2) and the GT^- amplitudes is of the order of 7 to 10. They are, of course, in phase, as it is expected from the structure of both transition operators. Hence, interaction between the GT^- and $IVSM^-$

TABLE IV. Energetics of the GT^- and $IVSM^-$ modes. The quantities E_{max} and $E_{centroid}$ are the energy of the state with the largest intensity and the energy centroid of the intensity distribution of each mode. All values are expressed in units of MeV. The two adopted occupancy schemes for ^{76}Ge have been indicated by "WS + BCS" and "exp".

Nucleus	$E_{max}(GT^-)$	$E_{centroid}(GT^-)$	$E_{max}(IVSM^-)$	$E_{centroid}(IVSM^-)$
^{76}Ge (WS + BCS)	15.312	12.816	31.642	24.659
^{76}Ge (exp)	15.397	12.588	29.089	23.268
^{82}Se	15.713	13.701	31.395	24.500
^{100}Mo	13.347	12.950	31.613	25.729
^{116}Cd	14.726	14.563	33.917	28.057
^{128}Te	14.409	12.564	30.228	23.868
^{130}Te	14.720	13.364	31.294	24.592
^{136}Xe	16.960	15.604	32.796	26.500

TABLE V. Intensity of the GT^- and $IVSM^-$ modes. The quantitity S_{max} is the intensity carried by the state of energy E_{max}, and S_{total} is the total intensity of each mode. The intensities corresponding to the IVSM mode are given in units of fm^4. The two adopted occupancy schemes for ^{76}Ge have been indicated by "WS + BCS" and "exp".

Nucleus	$S_{max}(GT^-)$	$S_{total}(GT^-)$	$S_{max}(IVSM^-)$	$S_{total}(IVSM^-)$
^{76}Ge (WS + BCS)	17.683	36.535	1.358×10^3	5.953×10^3
^{76}Ge (exp)	17.258	38.358	1.131×10^3	6.104×10^3
^{82}Se	27.589	42.309	1.999×10^3	6.411×10^3
^{100}Mo	21.889	50.287	3.771×10^3	1.580×10^4
^{116}Cd	15.786	60.528	5.577×10^3	2.232×10^4
^{128}Te	25.988	72.613	8.002×10^3	2.489×10^4
^{130}Te	23.564	78.404	7.623×10^3	2.646×10^4
^{136}Xe	37.696	84.249	8.780×10^3	2.369×10^4

TABLE VI. Energetics of the GT^+ and $IVSM^+$ modes. The quantities E_{max} and $E_{centroid}$ are the energy of the state with the largest intensity and the energy centroid of the intensity distribution of each mode. All values are expressed in units of MeV. The two adopted occupancy schemes for ^{76}Se have been indicated by "WS + BCS" and "exp".

Nucleus	$E_{max}(GT^+)$	$E_{centroid}(GT^+)$	$E_{max}(IVSM^+)$	$E_{centroid}(IVSM^+)$
^{76}Se (WS + BCS)	8.093	10.551	27.173	22.712
^{76}Se (exp)	7.313	8.727	25.612	22.519
^{82}Kr	8.158	11.146	27.042	22.293
^{100}Ru	3.507	4.830	21.209	19.800
^{116}Sn	2.515	6.907	26.284	22.271
^{128}Xe	6.468	10.895	23.613	21.040
^{130}Xe	8.009	12.604	22.187	19.559
^{136}Ba	6.912	10.866	21.225	18.834

TABLE VII. Intensity of the GT^+ and $IVSM^+$ modes. The quantitity S_{max} is the intensity carried by the state of energy E_{max}, and S_{total} is the total intensity of each mode. The intensities corresponding to the IVSM mode are given in units of fm^4. The two adopted occupancy schemes for ^{76}Se have been indicated by "WS + BCS" and "exp".

Nucleus	$S_{max}(GT^+)$	$S_{total}(GT^+)$	$S_{max}(IVSM^+)$	$S_{total}(IVSM^+)$
^{76}Se (WS + BCS)	0.386	1.161	1.155×10^3	5.841×10^3
^{76}Se (exp)	1.788	3.400	2.212×10^3	5.940×10^3
^{82}Kr	0.353	0.909	2.506×10^3	6.397×10^3
^{100}Ru	3.597	3.975	4.486×10^3	9.489×10^3
^{116}Sn	1.350	5.031	6.328×10^3	1.413×10^4
^{128}Xe	0.340	1.051	6.785×10^3	1.267×10^4
^{130}Xe	0.271	0.701	6.388×10^3	1.229×10^4
^{136}Ba	0.322	0.543	7.274×10^3	1.274×10^4

TABLE VIII. Amplitudes of the GT^- and $IVSM^-$ transitions, given in the last two columns, from the ground states of the nuclei of column 1 to the $J^\pi = 1^+$ states of the nuclei listed in column 2. Listed are the amplitudes of transitions to states around the GTGR with a magnitude of the GT^- amplitude larger than unity. The third column gives the pnQRPA energy. For ^{76}Ge both the "WS + BCS" occupancies and the "exp" occupancies are used in the calculations.

0^+_{gs}	1^+ states of	Energy (MeV)	GT amplitude	IVSM amplitude (fm^2)
		11.424	−2.148	−6.693
^{76}Ge	^{76}As	14.118	−1.264	−9.138
(WS + BCS)	(WS + BCS)	15.312	4.205	29.028
		10.540	2.032	6.106
^{76}Ge	^{76}As	15.314	−1.800	−13.015
(exp)	(exp)	15.396	4.154	30.376
^{82}Se	^{82}Br	15.713	−5.252	−36.716
		13.346	4.678	40.322
^{100}Mo	^{100}Tc	13.558	−3.521	−28.504
		17.735	1.628	16.328
		10.874	1.490	16.914
		11.372	−1.657	−14.316
		14.726	3.973	32.826
^{116}Cd	^{116}In	14.900	−2.565	−19.936
		16.328	−1.834	−21.528
		16.798	−1.359	−13.731
		16.954	−1.339	−14.568
		17.119	3.341	33.131
		6.197	−1.196	−12.633
		6.303	−1.127	−9.330
		7.306	2.415	23.256
^{128}Te	^{128}I	9.569	3.475	21.813
		14.322	−2.282	−24.011
		14.409	5.097	55.070
		14.685	−1.794	−16.353
		14.692	−2.672	−25.255
		14.293	2.160	24.671
^{130}Te	^{130}I	14.719	4.854	48.815
		14.880	4.794	49.351
		16.795	4.868	46.136
^{136}Xe	^{136}Cs	16.960	−6.139	−59.075
		17.595	−1.443	−14.118

modes is likely and it may induce a shift to lower energies of some of the spin-isospin strength carried by the $IVSM^-$ mode, as predicted by the perturbative analysis of Ref. [9], performed in the context of a schematic model. This could have significant effects for the experimental analysis of the GT^- strength at the GTGR energies.

Concerning the differences caused by the two occupation schemes used for the $A = 76$ triplet of isobars we notice from Fig. 1 and Tables IV and V that no drastic differences are observed with the resulting GT^- and $IVSM^-$ distributions of strength. The GT^- distributions are quite similar, as is also indicated by the cumulative sum of Fig. 9, but there is some strength redistribution for the $IVSM^-$ strength when going from the "WS + BCS" to the "exp" occupancies. For the GT^+ and $IVSM^+$ strength distributions a stronger effect appears, as noticed from Fig. 2 and Tables VI and VII. In particular the total and peak GT^+ strengths are drastically increased when going from the "WS + BCS" to the "exp" occupancies. The total $IVSM^+$ strength is not much affected by going from one occupancy scheme to the next but there is some redistribution of strength at the main peak.

Finally, in Fig. 10 we show the mass dependence of the total effective GT^- and GT^+ strengths (left panel) and the total effective strengths of the $IVSM^\pm$ transitions (right panel) taken from Tables V and VII. The GT results of Fig. 10 agree with the Ikeda $3(N - Z)$ sum rule. The interesting thing about the IVSM modes is that the total $IVSM^-$ strength has a much steeper slope than the total $IVSM^+$ strength as a function of the mass number A. This makes the difference of the strengths an increasing function of A. As already noted earlier, for the $A = 76$ isobars the results with the BCS and experimental occupancies do not deviate notably from each other in the case of the IVSM strengths. For the GT^+ strength the relative difference is notable.

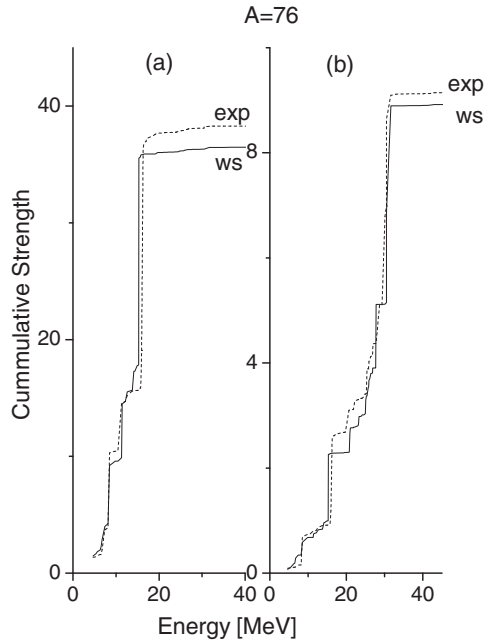

FIG. 9. Cumulative sums of the effective GT^- strength (6) [left panel] and $IVSM^-$ strength (8) [right panel] for the transition $^{76}Ge \rightarrow {}^{76}As$ calculated by using the "WS + BCS" and the "exp" occupancies. The excitation energies are measured from the ground state of ^{76}Ge. The IVSM strength is normalized by dividing by R^4 where $R = 5.08$ fm is the nuclear radius.

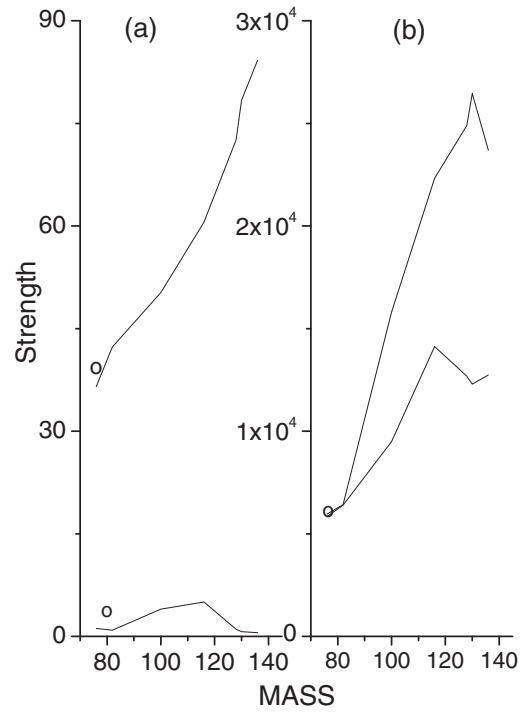

FIG. 10. Left panel: The total effective GT^- (upper curve) and GT^+ (lower curve) strengths, (6) and (7), as functions of the mass number. Right panel: The total effective $IVSM^-$ (upper curve) and $IVSM^+$ (lower curve) strengths, (8) and (9), as functions of the mass number in units of fm^4. The small circles indicate the results obtained with the "exp" occupancies for the $A = 76$ nuclei. For the IVSM the circles coincide in the scale of the figure (see also Tables V and VII).

IV. CONCLUSIONS

In this work we have performed realistic pnQRPA calculations of the GT and IVSM excitations in double-odd mass nuclei, which belong to double-beta-decay triplets with $A = 76$, $A = 82$, $A = 100$, $A = 116$, $A = 128$, $A = 130$, and $A = 136$. The calculations were performed in large single-particle bases with realistic Bonn-A based two-body interactions. We have fitted the observed odd-even mass differences by adjusting the couplings of the pairing monopole channels separately for protons and neutrons. Similarly, we have fitted the energy of the GTGR centroids by varying the parameters entering the proton-neutron particle-hole channel of the pnQRPA. The systematics shows that the IVSM and GT modes may be correlated, and that the presence of strength, due to the t^- side of the IVSM excitations at energies near that of the GT^- giant resonance may be significant for double-beta-decay and (p,n)-type of reaction studies.

The overall picture which emerges from these calculations seems to stress the need of a detailed exploration of the region of excitations between 10 to 20 MeV in the odd-odd nuclei which are members of double-beta-decay triplets. There the presence of (p,n) strength may be partly due to excitations of the type $\sigma r^2 t^-$.

ACKNOWLEDGMENTS

This work has been partially supported by the CONICET (Argentina) and by the Academy of Finland under the Finnish Centre of Excellence Programme 2012–2017 (Nuclear and Accelerator Based Programme at JYFL).

[1] J. Maalampi and J. Suhonen, Adv. High. Energy Phys. **2013**, 505874 (2013).
[2] J. Suhonen and O. Civitarese, Phys. Rep. **300**, 123 (1998).
[3] J. Suhonen and O. Civitarese, J. Phys. G: Nucl. Part. Phys. **39**, 085105 (2012).
[4] J. Suhonen and O. Civitarese, J. Phys. G: Nucl. Part. Phys. **39**, 124005 (2012).
[5] J. Suhonen and O. Civitarese, Nucl. Phys. A **924**, 1 (2014).
[6] J. Suhonen and O. Civitarese, Nucl. Phys. A **847**, 207 (2010).
[7] J. Suhonen, Int. J. Mod. Phys. E **20**, 451 (2011).
[8] J. Suhonen, Nucl. Phys. A **853**, 36 (2011).
[9] D. R. Bes, O. Civitarese, and J. Suhonen, Phys. Rev. C **86**, 024314 (2012).
[10] S. Rakers *et al.*, Phys. Rev. C **71**, 054313 (2005).
[11] E. W. Grewe and D. Frekers, Prog. Part. Nucl. Phys. **57**, 260 (2006).
[12] E. W. Grewe *et al.*, Phys. Rev. C **76**, 054307 (2007).
[13] E. W. Grewe *et al.*, Phys. Rev. C **78**, 044301 (2008).

[14] H. Dohmann *et al.*, Phys. Rev. C **78**, 041602(R) (2008).
[15] M. Sasano *et al.*, in *Workshop on Matrix Elements for Double-beta-decay EXperiments (MEDEX)*, June 2009, Prague, edited by O. Civitarese, I. Stekl, and J. Suhonen, AIP Conf. Proc. No. 1180 (AIP, New York, 2009), p. 102.
[16] M. Sasano *et al.*, Phys. Rev. C **85**, 061301 (2012).
[17] A. Bohr and B. R. Mottelson, *Nuclear Structure, Vol. I* (Benjamin, New York, 1969).
[18] K. Holinde, Phys. Rep. **68**, 121 (1981).
[19] J. Suhonen, *From Nucleons to Nucleus: Concepts of Microscopic Nuclear Theory* (Springer, Berlin, 2007).
[20] J. Suhonen, Nucl. Phys. A **563**, 205 (1993).
[21] J. Suhonen, T. Taigel, and A. Faessler, Nucl. Phys A **486**, 91 (1988).
[22] I. Hamamoto and H. Sagawa, Phys. Rev. C **62**, 024319 (2000).
[23] J. Suhonen, Nucl. Phys. A **700**, 649 (2002).
[24] J. P. Schiffer *et al.*, Phys. Rev. Lett. **100**, 112501 (2008).
[25] B. P. Kay *et al.*, Phys. Rev. C **79**, 021301(R) (2009).
[26] J. Suhonen and O. Civitarese, Phys. Lett. B **668**, 277 (2008).
[27] M. Aunola and J. Suhonen, Nucl. Phys. A **602**, 133 (1996).
[28] M. Aunola and J. Suhonen, Nucl. Phys. A **643**, 207 (1998).
[29] J. Suhonen and M. Aunola, Nucl. Phys. A **723**, 271 (2003).
[30] J. Suhonen, Nucl. Phys. A **864**, 63 (2011).
[31] O. Civitarese, A. Faessler, and T. Tomoda, Phys. Lett. B **194**, 11 (1987).
[32] F. Šimkovic, A. Faessler, V. Rodin, P. Vogel, and J. Engel, Phys. Rev. C **77**, 045503 (2008).
[33] M. Kortelainen, O. Civitarese, J. Suhonen, and J. Toivanen, Phys. Lett. B **647**, 128 (2007).
[34] M. Kortelainen and J. Suhonen, Phys. Rev. C **75**, 051303(R) (2007).
[35] M. Kortelainen and J. Suhonen, Phys. Rev. C **76**, 024315 (2007).
[36] J. Suhonen and M. Kortelainen, Int. J. Mod. Phys. E **17**, 1 (2008).
[37] J. Suhonen, Phys. Lett. B **607**, 87 (2005).
[38] J. Suhonen and O. Civitarese, Phys. Lett. B **725**, 153 (2013).
[39] J. Kotila, J. Suhonen, and D. S. Delion, J. Phys. G **36**, 045106 (2009).
[40] O. Civitarese and J. Suhonen, Phys. Rev. C **58**, 1535 (1998).
[41] O. Civitarese and J. Suhonen, Nucl. Phys. A **653**, 321 (1999).